Colloids and Surfaces A: Physicochemical and Engineering Aspects 722 (2025) 137239

Contents lists available at ScienceDirect

Colloids and Surfaces A: Physicochemical and Engineering Aspects

journal homepage: www.elsevier.com/locate/colsurfa

Triphenylamine-linked triazine (D-A) units based hypercrosslinked porous polymer: Rapid adsorption and enhanced photodegradation of organic dyes from water

Mohsin Ejaz [a], Mohamed Gamal Mohamed [a,b,*], Mohammed G. Kotp [a], Ahmed M. Elewa [c], Shiao-Wei Kuo [a,d,*]

[a] Department of Materials and Optoelectronic Science, Center for Functional Polymers and Supramolecular Materials, National Sun Yat-Sen University, Kaohsiung 804, Taiwan
[b] Chemistry Department, Faculty of Science, Assiut University, Assiut 71515, Egypt
[c] Department of Chemical Engineering, National Tsing Hua University, Hsinchu 300044, Taiwan
[d] Department of Medicinal and Applied Chemistry, Kaohsiung Medical University, Kaohsiung 807, Taiwan

HIGHLIGHTS

- Donor-acceptor TPA-TAZ HPP was developed for adsorption and photocatalytic degradation of organic dyes.
- The TPA-TAZ HPP demonstrated excellent rapid removal efficiencies of approximately 99 % for both RhB and MB within 5 mins.
- The TPA-TAZ HPP exhibited adsorption capacities of up to 951 mg g^{-1} for RhB and 858 mg g^{-1} for MB.
- The TPA-TAZ HPP exhibited excellent photocatalytic degradation of RhB and MB, respectively.

GRAPHICAL ABSTRACT

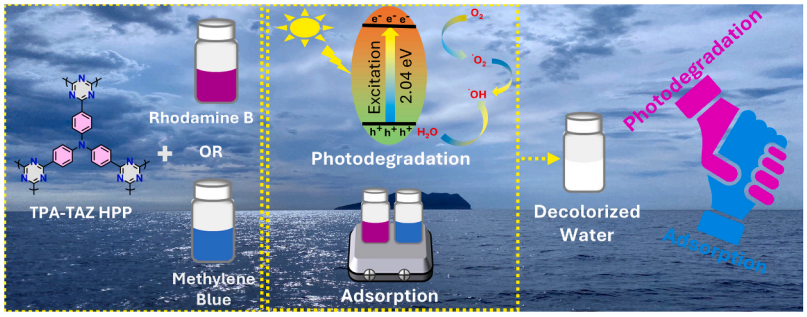

ARTICLE INFO

Keywords:
Hypercrosslinked porous polymer
Dyes adsorption
Photodegradation
Rhodamine B
Methylene Blue

ABSTRACT

Pigments and dyes are prevalent water contaminants, necessitating effective treatment methods. Hypercrosslinked porous polymers (HPPs), known for their high surface area and abundant micropores, effectively adsorb dye molecules and facilitate their degradation under light, making them a highly attractive solution. Herein, we synthesized donor-acceptor (DA) based TPA-TAZ HPP through Friedel–Crafts polymerization of triphenylamine as a donor and 2,4,6-trichloro-1,3,5-triazine (TCT) as an acceptor for adsorption and photodegradation of Rhodamine B (RhB) and methylene blue (MB). The resulting TPA-TAZ HPP exhibits an impressive surface area of 1823 m^2 g^{-1}, significant thermal stabilities (T_{d5}: 663 °C, T_{d10}: 674 °C, char yield: 75 wt%), and a small band gap of up to 2.04 eV. The porous framework, abundant adsorption sites, and electronegative characteristics of TPA-TAZ HPP enable it to achieve outstanding adsorption performance. It demonstrated removal efficiencies of nearly 99 % for both RhB and MB within 5 minutes, with remarkable adsorption capacities of up to 951 mg g^{-1} for RhB and 858 mg g^{-1} for MB at ambient temperature. Additionally, TPA-TAZ HPP

* Corresponding authors at: Department of Materials and Optoelectronic Science, Center for Functional Polymers and Supramolecular Materials, National Sun Yat-Sen University, Kaohsiung 804, Taiwan.
E-mail addresses: mgamal.eldin12@yahoo.com, mgamal.eldin12@aun.edu.eg (M.G. Mohamed), kuosw@faculty.nsysu.edu.tw (S.-W. Kuo).

https://doi.org/10.1016/j.colsurfa.2025.137239
Received 10 March 2025; Received in revised form 2 May 2025; Accepted 15 May 2025
Available online 22 May 2025

exhibited exceptional photocatalytic degradation efficiencies, achieving up to 88 % for RhB and 96 % for MB, with reaction rate constants of 5.78×10^{-2} min^{-1} and 9.62×10^{-2} min^{-1}, respectively. The superior performance of TPA-TAZ HPP can be attributed to its high surface area, small band gap, and donor-acceptor framework, which collectively facilitate efficient charge transfer, thereby enhancing both adsorption and photocatalytic degradation. Our findings suggest that this research could guide the effective design of donor–acceptor-based HPPs as promising photocatalysts for a wide range of photocatalytic applications.

1. Introduction

The advancement of pharmaceutical sectors in recent years has produced substantial contaminants that result in worldwide pollution of surrounding water and pose significant threats to the ecosystem and our health [1–5]. Organic dyes are the most prevalent and detrimental due to their extensive use in the printing, fabric, beauty products, wood, and pigment industries, as well as their irreversible harm to the human reproductive system, potentially elevating the risk of cancer [6–10]. Consequently, the purification of water, particularly the effective elimination of dyes, has emerged as a pressing issue necessitating collaborative efforts from scientists globally. At present, many removal methods such as photocatalysis [11,12], membrane filtering [13,14], biological therapy [15,16], and adsorption [17,18] have been implemented. Adsorption has garnered increasing global interest and acknowledgment due to its distinctive features, such as excellent elimination rate, cheap price, and ease [19]. The predominant adsorbents are porous substances, including porous organic polymers (POPs) [20], metal-organic frameworks (MOFs) [21], activated carbons [22], and bio-composite microspheres [23]. Nonetheless, the drawbacks, such as synthesis challenges, elevated costs, instability, poor adsorption efficiency, and capacity, have significantly hindered the advancement of the aforementioned adsorbents. Therefore, investigating innovative porous adsorbents characterized by ease of manufacture, cost-effectiveness, elevated adsorption efficiency, and recycling should be a prioritized research focus.

POPs are a novel category of porous materials that have garnered significant interest in both academic and industrial sectors. Due to their remarkable attributes, including synthetic variety, extensive specific surface area, substantial pore volume, exceptional thermal and chemical durability, ease of functionalization, high porosity, varied composition, and low density [24–28]. Hypercrosslinked porous polymers (HPPs) are classified as a type of POPs and are significant due to their benefits, which encompass facile functionalization, strategic monomer selection, elevated surface area, regulated reaction conditions, diverse synthetic methods, exceptional thermal stability, economical reagents, remarkable chemical resilience, and suitable crosslinker lengths to yield porous structures with a well-defined polymer framework [29–33]. The Friedel–Crafts chemistry approach is primarily used to synthesize HPPs, facilitating rapid kinetics to establish robust links and yielding a strongly crosslinked network with tailored porosity structure. Consequently, HCPs may serve as effective photocatalysts in diverse chemical processes, including photodegradation and photocatalytic water splitting [34–37]. The dual roles of HPPs photocatalysts and adsorbents for the removal of dyes can enhance their efficacy in wastewater treatment; however, the efforts continue to face challenges in optimizing the properties of HCPs to accommodate these dual functions with increased kinetic rates. The utilization of POPs as photocatalysts is restricted by elevated exciton binding energies and diminished charge carrier transport, leading to inadequate photocatalytic performance [38–40]. Nonetheless, these issues are tackled if donor-acceptor (D-A) framework polymers with intrinsic microporosity (POPs) are synthesized. The synthesis of D-A-based POP could be very effective owing to its capacity to exhibit intramolecular transfer charges induced by photonics interaction, rendering it appropriate for photocatalysis [41–43]. The integration of donor-acceptor moieties improves charge dissociation by diminishing exciton binding strength, resulting in an improvement in catalysis [44,45]. POPs have been examined for their ability to photocatalytically degrade organic contaminants [46–48]. Consequently, the development of environmentally acceptable donor and acceptor POPs for the photocatalytic degradation of the organic colors in water remains a challenge.

2,4,6-Trichloro-1,3,5-triazine (TCT), referred to as cyanuric chloride, is an intriguing chemical that mimics aromatic benzene, including alternating carbon and nitrogen atoms with three chlorine substituents on the carbon atoms. The prevalence of the basic triazine group (electron acceptor) facilitates diverse interactions with pollutants, making them a viable and regenerating polymer for many applications, including photocatalysts and absorbents [49]. Triphenylamine (TPA) derivatives (electron donor) exhibit exceptional characteristics, including increased aromaticity, redox capabilities, enhanced charge carrier mobility, and notable electronic properties. TPA-based POPs have strong performance in adsorption or photocatalysis [50]. To our knowledge, the photophysical characteristics of TPA-TAZ (D-A) based HPP have not been documented. Connecting with electron-rich monomers may create donor-acceptor complexes, enhancing the electrical and photophysical characteristics. Moreover, their adsorption properties and photocatalytic efficacy for the elimination of organic dyes have not been previously evaluated. Herein, we successfully synthesized HPP by Friedel−Crafts polymerization of TPA and TCT using $FeCl_3$ to afford TPA-TAZ HPP [Fig. 1 (a)]. The TPA-TAZ HPP was further utilized for adsorption and photodegradation of rhodamine B (RhB) and methylene blue (MB).

2. Materials

Triphenylamine (TPA), 2,4,6-trichloro-1,3,5-triazine (TCT), anhydrous ferric chloride ($FeCl_3$), and methanesulfonic acid (CH_3SO_3H) were purchased from Sigma Aldrich. Tetrahydrofuran (THF), 1,2-dichlorobenzene (DCB), acetone, and methanol were purchased from Acros.

2.1. Synthesis of TPA-TAZ HPP

TPA (0.7 g, 0.0028 mmol), TCT (1.6 g, 0.0086 mmol), and $FeCl_3$ (1.76 g, 0.010 mmol) were added to a reaction flask and evacuated under vacuum with nitrogen four times to remove any residual air. Subsequently, 40 mL of dichlorobenzene was introduced into the flask, and the reaction mixture was refluxed under N_2 for three days. After completion, the reaction mixture was allowed to cool, and the resulting solid product was collected by filtration and sequentially washed with tetrahydrofuran (THF), methanol, and acetone to remove any unreacted reagents or by-products. The solid was then dispersed in methanol and stirred at 70 °C for 1 hr to enhance purification. Finally, the solid was filtered and dried, yielding TPA-TAZ HPP as a fine powder (0.5 g, 86 %).

2.2. Dyes adsorption

The RhB and MB can be conveniently monitored using a standard UV–visible spectrophotometer, they were used to study the adsorption performance of TPA-TAZ HPP [51]. Firstly, 2 mg of TPA-TAZ HPP to 10 mL of dye solution (50 mg L^{-1}), which was then gently stirred at 1000 rpm with a pH of 7 and a temperature of 298 K. Using a centrifuge set at 4000 rpm for 5 minutes, we monitored the dyes concentration changes at regular intervals after the separation of TPA-TAZ HPP.

Kinetic isotherm curves were computed based on different dye concentrations (50–300 mg L^{-1}). As a result, 10 mL of a certain dye concentration was mixed with 2 mg of TPA-TAZ HPP separately, and the mixture was stirred for 24 hours. The kinetics and adsorption isotherms were realistically investigated using Langmuir models. The Langmuir isothermal model was used to determine the adsorption isotherms, which is shown in Equation S1.

2.3. Dyes photodegradation

Photodegradation experiments were conducted by dispersing 3 mg of TPA-TAZ HPP in 60 mL of an aqueous dye solution (75 mg L^{-1}). The solution was stirred at 500 rpm in the dark for five hours to reach adsorption equilibrium. Subsequently, the mixture was exposed to visible light at room temperature for 330 minutes. Throughout the experiment, the concentration of the dye was monitored over time using UV-spectroscopy after separating the TPA-TAZ HPP [52]. A 450 nm optical filter was placed in front of the xenon lamp to eliminate UV-induced dye degradation, ensuring that only visible light contributed to the reaction. The distance between the light source and the dye solution was strictly maintained at 5 cm to ensure consistent irradiation intensity. Control experiments confirmed that dyes did not undergo degradation in the absence of either the TPA-TAZ HPP photocatalyst or visible light, demonstrating that both factors are essential for the photocatalytic process.

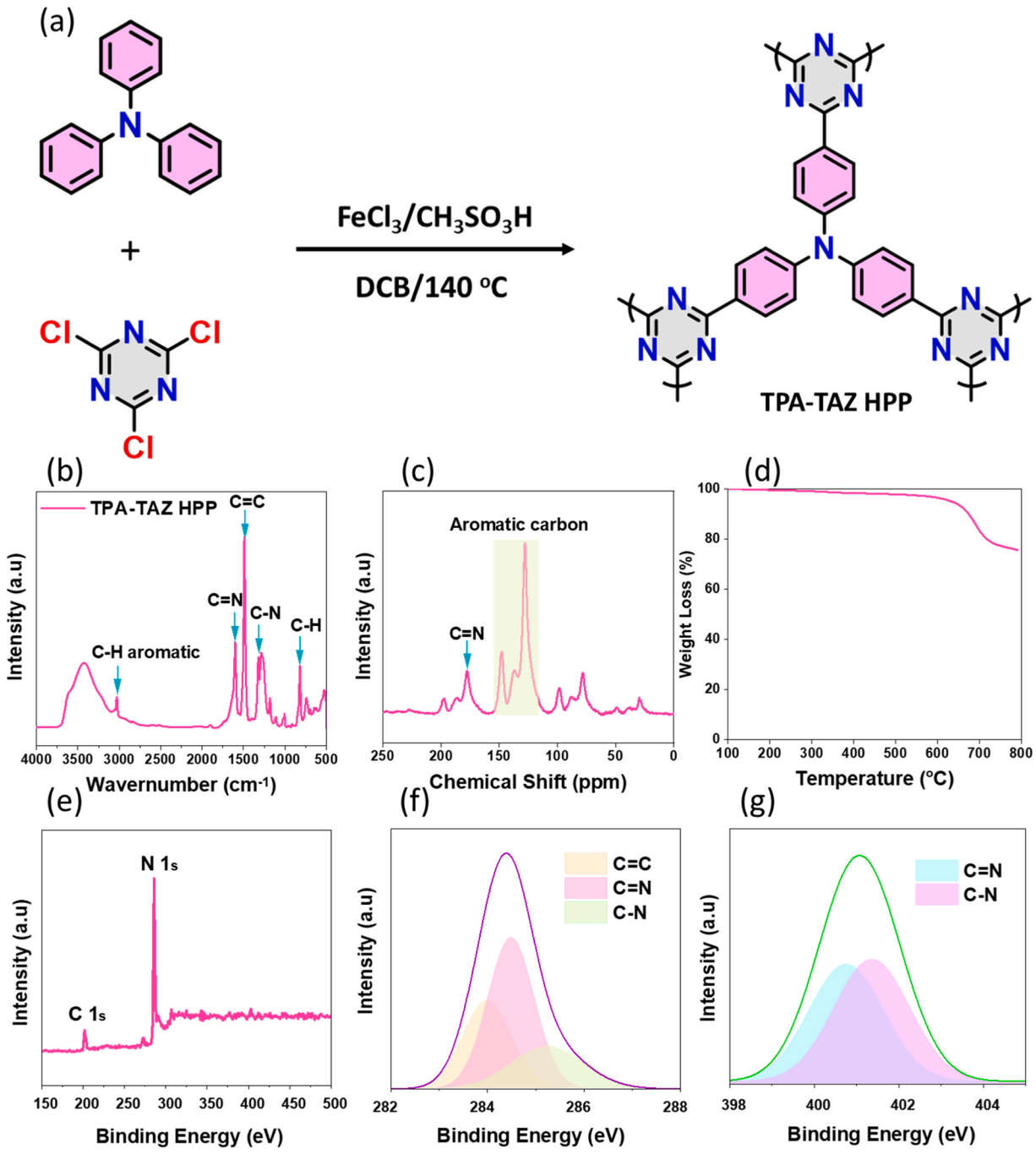

Fig. 1. (a) Synthesis route for TPA-TAZ HPP. (b) FTIR, (c) solid-state ^{13}C NMR, and (d) TGA profile of TPA-TAZ HPP. (e) XPS survey, (f) C 1 s, and (g) N 1 s spectra of TPA-TAZ HPP.

3. Results and discussion

3.1. Synthesis and characterization of TPA-TAZ HPP

The synthesis of TPA-TAZ HPP was synthesized via a Friedel–Crafts alkylation reaction between triphenylamine (TPA) and TCT in the presence of $FeCl_3$, methanesulfonic acid, and dichlorobenzene under reflux at 140 °C for three days [Fig. 1(a)]. The structure of TPA-TAZ HPP was confirmed using FTIR and solid-state NMR spectroscopy. In the FTIR spectrum, the characteristic absorption peaks were noticed at 3028 cm^{-1} (aromatic C–H stretching), 1600 cm^{-1} (C═N stretching), 1489 cm^{-1} (C═C stretching), 1320 cm^{-1} (C–N stretching), and 816 cm^{-1} (C–H bending of the triazine unit). Additionally, a broad peak at 3430 cm^{-1} indicates water adsorption due to the porous nature of TPA-TAZ HPP [Fig. 1(b)]. Solid-state ^{13}C NMR spectroscopy further confirmed the successful polymerization and high crosslinking density of TPA-TAZ HPP. The signals observed in the range of 120–139 ppm correspond to aromatic carbons, while peaks at 178 ppm and 148 ppm are attributed to C═N and C–N units, respectively, providing clear evidence of the presence of triazine groups within the polymer network [Fig. 1(c)].

The thermal stability of TPA-TAZ HPP was examined using thermogravimetric analysis (TGA). The TPA-TAZ HPP exhibited exceptional thermal resistance, with decomposition temperatures (T_{d5} and T_{d10}) of 663 °C and 674 °C, respectively, and a high char yield of 75 wt% at 800 °C [Fig. 1(d)]. This exceptional stability is attributed to the high crosslinking density of the monomers (TPA and TCT), the presence of thermally robust triazine units, and the rigid aromatic framework. X-ray diffraction (XRD) analysis revealed that TPA-TAZ HPP is amorphous in nature [Figure S1]. Further insights into the elemental composition were obtained through X-ray photoelectron spectroscopy (XPS) [Fig. 1(e)]. The C1s spectrum displayed three distinct peaks at 283.4 eV, 284.4 eV, and 285.24 eV, corresponding to C═C, C═N (triazine group), and C–N bonds, respectively [Fig. 1(f)]. The N1s spectrum showed two peaks at 400.76 eV and 401.37 eV, which can be assigned to N = C (aromatic triazine group) and N-$(C)_3$ linkages, respectively [53] [Fig. 1(g)]. These XPS results further confirm the successful synthesis of TPA-TAZ HPP.

The high surface area of POPs plays a critical role in enhancing their adsorption and photocatalytic performance. This is primarily due to the increased exposure of active sites and the facilitation of efficient charge transfer processes. To evaluate the porosity of TPA-TAZ HPP, nitrogen (N_2) adsorption-desorption isotherms were measured at 77 K [Figs. 2(a) and 2(b)]. The resulting isotherm exhibited a Type IV curve with an H_2 hysteresis loop, as classified by IUPAC [Fig. 2(a)]. This hysteresis loop is indicative of the material's unique pore structure, characterized by large cavities connected by narrow channels, often referred to as "ink-bottle" pores [54]. The steep adsorption and delayed desorption observed in the isotherm are consistent with this pore morphology, where nitrogen molecules are initially trapped in the larger cavities and subsequently released through the narrower necks [55]. The N_2 adsorption-desorption isotherm also revealed a rapid uptake of nitrogen at both low and high relative pressures, pointing to the existence of microporous and mesoporous features within the TPA-TAZ HPP framework [Fig. 2(a)]. The Brunauer-Emmett-Teller (BET) surface area of TPA-TAZ HPP was determined to be 1823 m^2 g^{-1}, with two distinct, narrow peaks at 1.14 and 1.83 nm, and a pore volume of 2.05 cm^3 g^{-1} [Fig. 2(b)]. These values indicate that TPA-TAZ HPP is predominantly microporous, with a complex pore morphology that contributes to its high surface area. Such characteristics are often observed in materials with hierarchical porosity or highly interconnected network structures. The bulky, non-planar structure of TPA plays a significant role in enhancing the material's porosity. The three phenyl groups attached to the central nitrogen atom create steric hindrance, which prevents dense packing and promotes the formation of open, porous frameworks. This structural feature disrupts π–π stacking interactions, which are common in planar aromatic systems, thereby increasing the accessibility of voids and improving overall porosity [56]. Additionally, TPA's electron-donating properties enhance its reactivity in Friedel–Crafts reactions, enabling efficient cross-linking with tricarbonyl chloride (TCT). The combination of steric effects and reactivity results in a highly interconnected, crosslinked network. This increased cross-linking density generates a complex three-dimensional architecture, further amplifying the material's surface area. The morphology of TPA-TAZ HPP was further investigated using scanning

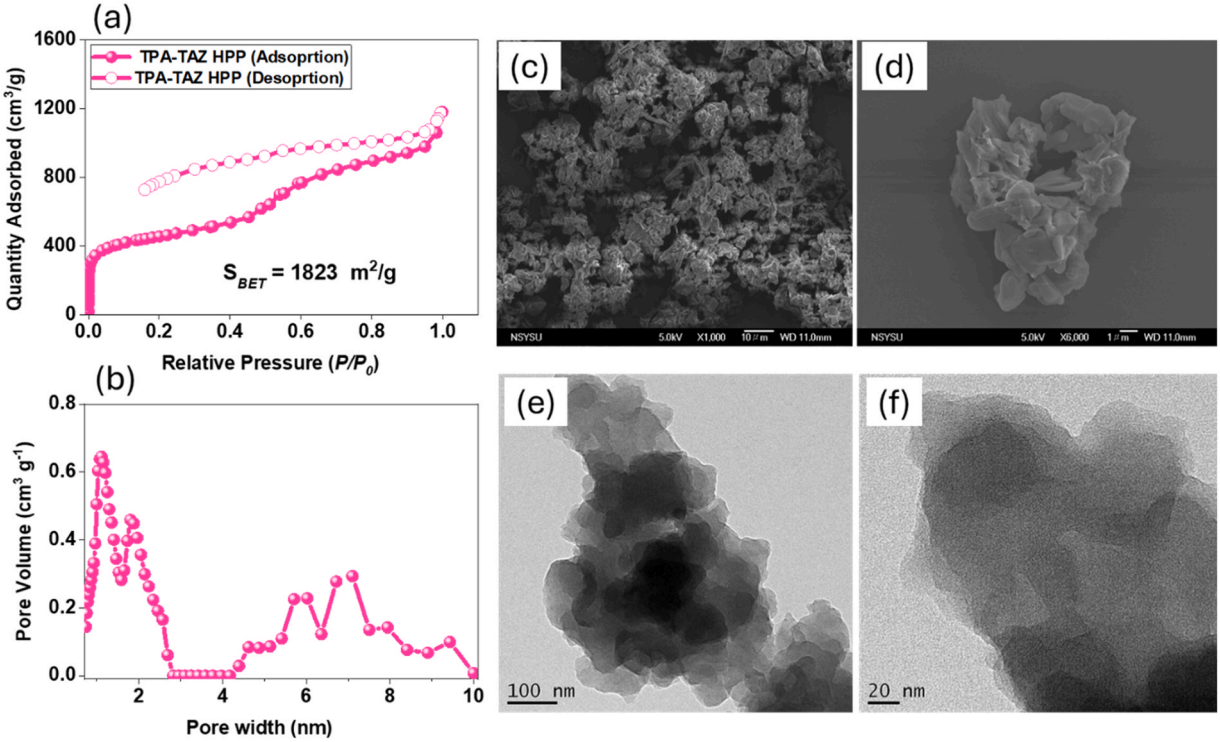

Fig. 2. (a) N_2 adsorption/desorption isotherms, (b) pore size (c-d) SEM, and (e-f) TEM images of TPA-TAZ HPP.

electron microscopy (SEM) and transmission electron microscopy (TEM) [Figs. 2(c) and 2(f)]. The SEM and TEM images revealed that the material is composed of aggregated spherical particles, which contribute to its high surface area and microporous nature. SEM mapping confirmed the uniform distribution of carbon (C) and nitrogen (N) throughout the TPA-TAZ HPP structure, as illustrated in Figure S2. In summary, the high surface area, hierarchical porosity, and interconnected network of TPA-TAZ HPP are attributed to the steric effects of TPA, its electron-donating properties, and the efficient cross-linking with TCT. These features make TPA-TAZ HPP a promising material for applications in adsorption and photocatalysis, where high surface area and efficient charge transfer are critical.

3.2. Optical properties of TPA-TAZ HPP

The photocatalytic efficiency of light-absorbing polymers is highly dependent on their physicochemical properties, particularly their ability to capture and utilize light energy [57]. Consequently, the optical properties of TPA-TAZ HPP were evaluated using UV–Visible spectroscopy and photoluminescence (PL) analysis [Fig. 3]. The UV–Visible absorption spectra revealed that TPA-TAZ HPP exhibits a strong visible-light absorption capability, with an absorption onset at 396 nm and an extended absorption tail reaching up to 800 nm [Fig. 3(a)]. This broad absorption range suggests that TPA-TAZ HPP can efficiently harness visible radiation, potentially enhancing its photocatalytic activity. Photocatalysis relies on the generation, separation, and migration of photo-induced electron-hole pairs. To further assess the electronic properties of TPA-TAZ HPP, the PL spectrum was recorded, showing a pronounced fluorescence peak at 466 nm [Fig. 3(b)]. Additionally, the optical band gap plays an important part in determining the extent of light absorption. Density functional theory (DFT) calculations were carried out to estimate the highest occupied molecular orbital (HOMO), lowest unoccupied molecular orbital (LUMO), and overall band gap energy of TPA-TAZ HPP [Fig. 3(c)]. The obtained values were −2.65 eV (HOMO), −0.61 eV (LUMO), and 2.04 eV (band gap). The relatively small band gap of TPA-TAZ HPP facilitates efficient visible-light absorption, which can enhance the degradation of organic dyes [58].

3.3. Dye adsorption performance of TPA-TAZ HPP

The adsorption of organic contaminants in aquatic environments can be influenced by several factors, including the existence of nitrogen-functionalized moieties, high charge density, and amine groups on the adsorbent materials. These features enhance the physical and chemical interactions between the sorbent and the contaminants. The active sites in polymers, which have enriched nitrogen moieties, strengthen the interaction among the dyes and the polymer. This interaction is stabilized by various non-covalent bonds [59]. POPs are known for their significant surface areas and porous structures, which facilitate the adsorption of dyes [60]. Our synthesized TPA-TAZ HPP demonstrates exceptional porosity, with surface areas reaching up to 1823 $m^2 g^{-1}$ and pore volumes as large as 2.05 $cm^3 g^{-1}$. We believe that TPA-TAZ HPP will serve as an effective organic adsorbent for removing harmful compounds from aquatic environments, a method that has proven more effective than other strategies. To assess the adsorption efficiency of TPA-TAZ HPP, we used synthetic dyes like rhodamine B (RhB) and methylene blue (MB) as model guest molecules at pH 7 and 298 K. The effectiveness of TPA-TAZ HPP in adsorbing RhB and MB was evaluated by monitoring the UV spectra. We concentrated on peak tracking variations in the highest adsorption peak at different time intervals (from 0 to 5 minutes) after adding 2 mg of TPA-TAZ HPP, stirred at 1000 rpm. The removal efficiency for RhB was 72.9 % and for MB was 69 % after stirring for 1 minute [Figs. 4(a) and 4(b)]. These values increased to 98 % for RhB and 95.8 % for MB after 4 minutes. A clear solution was observed for RhB after 5 minutes, while for MB, it took 6 minutes. This demonstrates that TPA-TAZ HPP exhibited excellent rapid adsorption performance for removing organic dyes from water [Figs. 4(c) and 4(d)]. Investigating adsorption isotherm models provides valuable insight into the adsorption behavior and performance of the adsorbent. Therefore, the RhB and MB solutions with concentrations ranging from 150–300 mg L^{-1} were prepared for adsorption analysis. For each concentration, 10 mL of the dye solution was combined with 2 mg of TPA-TAZ HPP and stirred continuously for 24 hours at a constant temperature to ensure equilibrium. The remaining dye concentration in each sample was quantified using UV–visible spectroscopy. The variation in adsorption capacity (Q_e) relative to equilibrium concentration (C_e) for both dyes interacting with TPA-TAZ HPP is illustrated in Figs. 4(e) and 4(f). A clear trend emerged, showing that higher initial dye concentrations resulted in greater adsorption capacities, which gradually stabilized as C_e increased. This can be attributed to the intensified concentration gradient at elevated dye levels, which improves molecular diffusion towards the TPA-TAZ HPP surface. Consequently, more dye molecules became adsorbed, confirming the strong affinity and adsorption efficiency of TPA-TAZ HPP for removing RhB and MB from water. The adsorption kinetics of the dyes by TPA-TAZ HPP were analyzed using the Langmuir isothermal model, and the comprehensive data is summarized in Table S1. The linear fitting of the Langmuir model showed high correlation coefficients (R^2) of 0.9998 for RhB and 0.9960 for MB [Fig. 4(e)]. TPA-TAZ HPP achieved maximum adsorption capacities (Q_m) of 951 mg/g for RhB and 858 mg/g for MB, with R_L values of 0.9762 and 0.9883, respectively [Fig. 4 (f)]. The adsorption capacities of our synthesized TPA-TAZ HPP towards RhB and MB are equivalent to, and in some cases exceed the maximum adsorption capacities of several previously reported porous materials (Table S2). The excellent

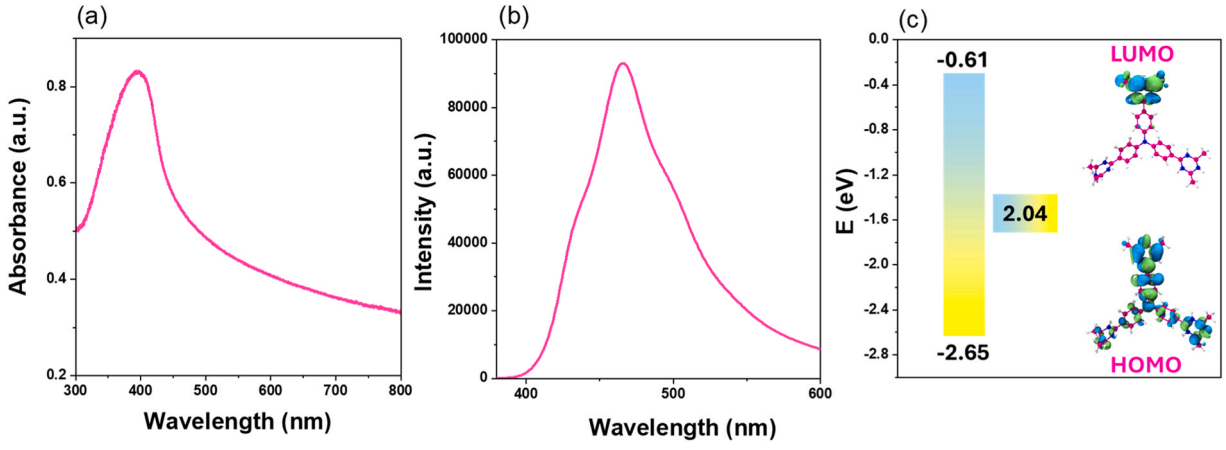

Fig. 3. (a) UV-Vis, and (b) PL spectra of TPA-TAZ HPP. (c) The schematic diagram for calculating the band gap of TPA-TAZ HPP.

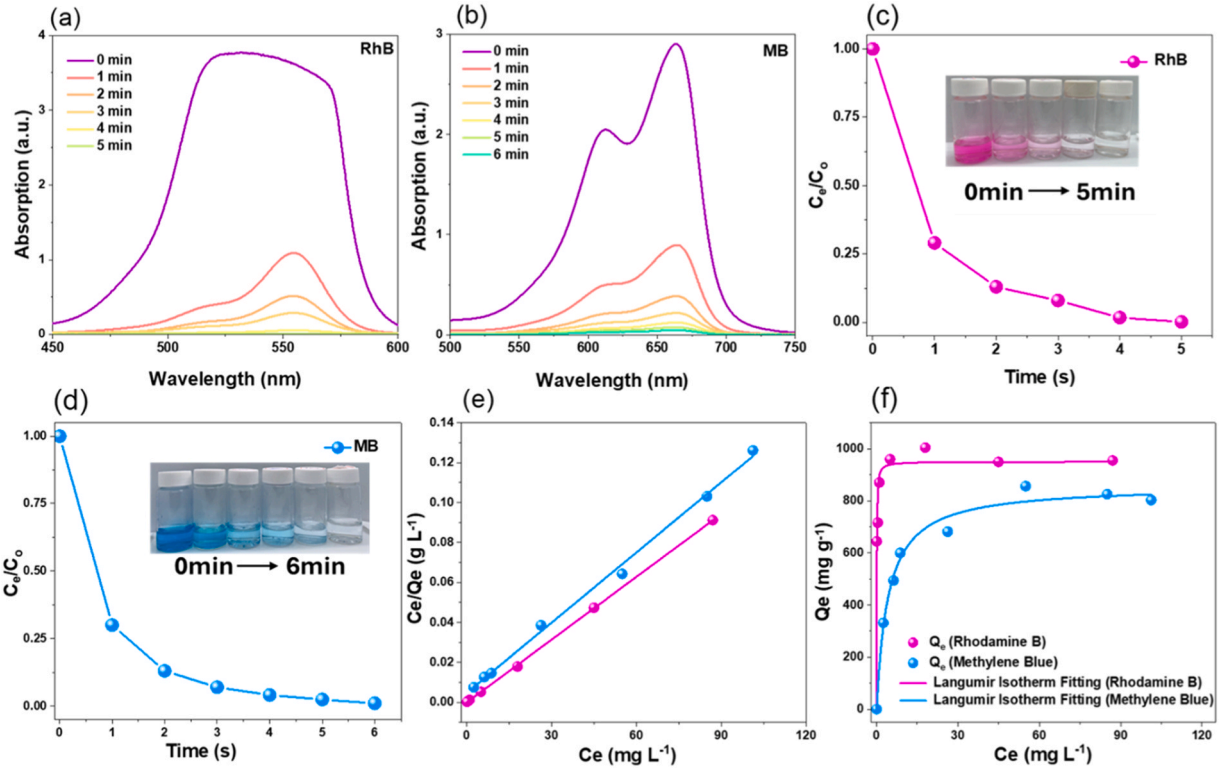

Fig. 4. (a) UV-Vis spectra of RhB dye solution, (b) UV-Vis Spectra of MB dye solution at different time intervals by adding TPA-TAZ HPP, (c) adsorption rates of RhB dye, (d) adsorption rates of MB dye, (e) adsorption isothermal curves of dyes onto TPA-TAZ HPP and (f) Langmuir isothermal models of dyes adsorption onto TPA-TAZ HPP.

adsorption properties of TPA-TAZ HPP are linked to various aspects, such as its high surface area, porosity, and both chemical and physical interactions, including π-π stacking with the dyes [61].

Boosting an adsorbent's pore volume and surface area has been shown to enhance the removal efficiency of organic dyes. The BET surface area of TPA-TAZ HPP is remarkably high (1823 $m^2 g^{-1}$), with a total pore volume of 2.05 $cm^3 g^{-1}$. The pore size distribution shows two narrow peaks at 1.14 and 1.83 nm, indicating hierarchical porosity. Despite the relatively large molecular size of RhB (~1.5–2.0 nm), the material demonstrates effective adsorption. This is primarily due to the hierarchical porosity of TPA-TAZ HPP, which facilitates better pore accessibility. While the 1.14 nm pores may partially restrict RhB diffusion, the presence of larger pores (1.83 nm) and possible interparticle voids or structural irregularities enables dye molecules to access internal active sites. In this context, the hierarchical pore structure plays a dominant role in overcoming size exclusion limitations, allowing for efficient adsorption of even bulky dyes. In contrast, MB has a smaller molecular size (~1.3 nm), which fits well within the pore size range of TPA-TAZ HPP. In both cases, the exceptionally high surface area provides many active adsorption sites, significantly enhancing the dye uptake capacity. Even if some micropores are not fully accessible to RhB, the synergy of hierarchical porosity and high surface area ensures strong adsorption performance for both dyes. In summary, the hierarchical porous structure of TPA-TAZ HPP facilitates efficient diffusion and adsorption of both RhB and MB, while the high surface area further amplifies the adsorption capacity by offering plentiful active sites. This makes TPA-TAZ HPP a highly effective adsorbent for a range of organic dyes, regardless of their molecular size. Previous studies have indicated that enhanced adsorption is often a result of increased π-π stacking interactions among the dyes and the adsorbent [46,57]. In this case, the aromatic triphenylamine and triazine units in TPA-TAZ HPP contribute significantly to its dye removal effectiveness. These units form stable and durable aromatic π-π stacking with dye molecules. To further investigate this interaction, we performed FTIR analysis before and after adsorption to explore the π-π stacking between TPA-TAZ HPP and the dyes (RhB and MB). Figures S3 and S4 illustrate that there are no significant alterations in the FTIR bands, a minor shift in the wavenumbers, thereby corroborating our prior assumption regarding the existence of interfacial contact (π-π stacking) among the adsorbent and dye molecules. Furthermore, the varying adsorption capabilities of TPA-TAZ HPP for dyes are attributable to the distinct molecular sizes of RhB (1.59 × 1.18 × 0.56 nm^3) and MB (1.26 × 0.77 × 0.65 nm^3). Due to its smaller size, MB is unable to be retained and may readily exit the pores, resulting in the lowest adsorption capacity of RhB. The bigger RhB molecules might block micropores and adhere to mesopores, leading to increased adsorption capabilities [61].

The adsorption behavior of Rhodamine B (RhB) and Methylene Blue (MB) was investigated at varying pH levels (2, 4, 6, and 7). For each experiment, 2 mg of TPA-TAZ HPP was dispersed in 10 mL of an aqueous dye solution (300 mg L^{-1}) and stirred gently at 1000 rpm for 24 hours at 298 K. The pH was adjusted accordingly, with pH 7 used as the reference condition [Figure S5]. Findings indicated a progressive improvement in adsorption efficiency as pH increased, peaking at pH 7. This trend can be attributed to two reasons: alterations in adsorbent surface charge and transformation in dye molecular properties. Under acidic conditions (low pH), the adsorbent surface undergoes significant protonation, acquiring a positive charge. Consequently, electrostatic repulsion occurs between the cationic dyes and the positively charged adsorbent, hindering adsorption. At higher pH levels, protonation diminishes, leading to a neutral or negatively charged surface. This change assists in electrostatic attraction, boosting dye uptake. Furthermore, the molecular state of Rhodamine B is pH-dependent. In acidic environments, it may adopt a zwitterionic or lactone configuration, weakening its adsorption affinity [10,17]. Near-neutral pH, however, it primarily exists in a cationic form, strengthening its interaction with the adsorbent. Methylene Blue, a permanently cationic heterocyclic compound,

exhibits a consistent positive charge but responds to surface charge variations. Its planar geometry and fixed cationic nature enhance adsorption as the adsorbent becomes more negatively charged at elevated pH. Ultimately, the synergistic influence of optimized surface charge and dye structural changes at higher pH levels maximizes adsorption efficiency at pH 7.

3.4. Photodegradation performance of TPA-TAZ HPP

Taking advantage of TPA-TAZ HPP's high surface areas, good porosity, photophysical properties, and narrow band gap, the photocatalytic activity was tested for degradation of RhB and MB in water through visible light. Control experiments were conducted to confirm the photocatalytic nature of the degradation. To ensure sufficient interaction between the adsorbent and dye molecules, we allowed the mixture to undergo adsorption in the dark for 5 hours before light irradiation [Figure S6]. This duration was selected to ensure that adsorption equilibrium was fully established under these experimental conditions. After 5 hours, dye molecules remained in the solution, indicating that adsorption alone could not achieve complete removal. Therefore, photodegradation was initiated to eliminate the residual dyes. When exposed to visible light (> 450 nm) for 120 minutes, the photodegradation efficiencies of RhB and MB on the TPA-TAZ HPP were found to be 47 % and 62 %, respectively [Figs. 5(a) and 5(b)]. The TPA-TAZ HPP demonstrated almost the degradation of RhB and MB molecules in 330 minutes [Fig. 5(c)], with photodegradation efficiencies of 88 % and 96 %, respectively [Fig. 5(e)]. The variation in degradation rates among the dyes may be attributed to their distinct molecular structures and adsorption characteristics on the photocatalyst [52]. Additionally, photocatalytic experiments using the individual components TPA and TCT were conducted under identical conditions for the degradation of methylene blue (MB). Both TPA and TCT exhibited significantly lower adsorption and degradation efficiencies compared to the synthesized TPA-TAZ HPP, highlighting the synergistic effect in the crosslinked framework [Figure S7]. Upon exposure to visible light (>450 nm) for 300 minutes, the photodegradation efficiencies of TPA and TAZ were found to be 38.1 % and 27.8 %, respectively, which are substantially lower than TPA-TAZ HPP under the same conditions. The inferior performance of the individual components can be attributed to their relatively low porosity and limited surface area, which restricts their dye adsorption capacities. In contrast, the crosslinked TPA-TAZ HPP exhibits a high surface area (1800 m^2/g), enhancing dye adsorption and facilitating efficient photocatalytic degradation. These results confirm that the superior photocatalytic performance of the HPP arises from both the synergistic interaction between TPA and TCT and the enhanced porosity of the resulting framework. These findings show that the recently synthesized TPA-TAZ HPP has exceptional photocatalytic properties for breaking down MB and RhB in the presence of visible light. High surface area, lower band gap, and a donor-acceptor framework are believed to be responsible for the enhanced performance of RhB and MB photodegradation over TPA-TAZ HPP. The increase of active sites may be accelerated by the large surface area. As a result, a large surface area (1823 m^2 g^{-1}) with amorphous structures may generate high defect concentrations, which in turn improve exciton dissociation and increase polymer photocatalytic performance. Furthermore, under the influence of light, holes and electrons may be produced in semiconductors during photocatalytic reactions. However, the photocatalysis process was significantly hampered by the quick recombination of electrons and holes. The donor-acceptor system generated an internal electric field inside the photocatalyst, facilitating the dissociation of excitons into free electrons and holes [47]. Therefore, TPA-TAZ HPP, having a donor-acceptor configuration, can efficiently promote photodegradation efficiency. The role of the donor-acceptor framework in charge separation and transfer was further proven by Time-resolved photoluminescence (TRPL) measurements. We conducted TRPL measurements on the individual donor (TPA) and acceptor (TCT) monomers, as well as the resulting polymer (TPA-TAZ HPP) [Figure S8]. The TRPL analysis revealed that TPA exhibited a longer PL

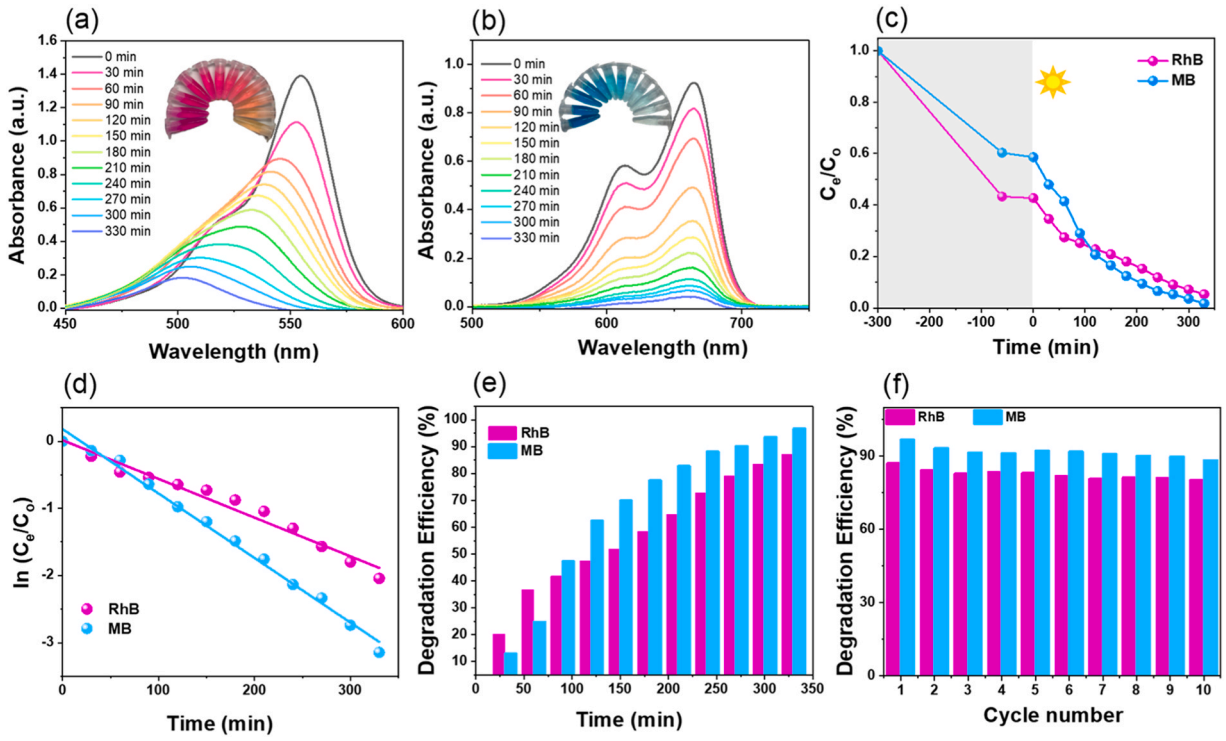

Fig. 5. (a) UV-Vis spectra of photocatalytic degradation of RhB, (b) UV-Vis spectra of photocatalytic degradation of MB dye solution at different time intervals by adding TPA-TAZ HPP, (c) photocatalytic rates of dyes, (d) Pseudo-first-order kinetic curves for the photodegradation for dyes, (e) photodegradation efficiencies of dyes and (f) photodegradation cycling of dyes.

decay lifetime, whereas the acceptor monomer displayed a significantly shorter lifetime. Notably, the TPA-TAZ HPP demonstrated an intermediate lifetime, positioned between those of the TPA and TCT. This observation suggests a synergistic interaction between the TPA and TCT units within the TPA-TAZ HPP backbone. The intermediate decay lifetime of the TPA-TAZ HPP implies that photoexcitation induces partial charge separation due to the donor-acceptor structural arrangement. This leads to suppressed radiative recombination compared to the donor monomer, yet not as rapid as the quenching observed in the acceptor. These findings support the presence of intramolecular charge transfer interactions within the polymer, which enhance charge separation efficiency relative to the isolated monomers. The Langmuir–Hinshelwood model ($\ln(C_o/C_t) = kt$) was used to carry out and evaluate the kinetic study of the photocatalytic degradation of TPA-TAZ HPP. In this model, C_o denotes the initial concentration of the dyes, C_t denotes the dye concentration at time t (min), k is the reaction rate constant, and t is the duration (min) of UV–vis light irradiation. The Langmuir-Hinshelwood models for RhB and MB were fitted using pseudo-first-order kinetics, as shown in [Fig. 5(d)]. Linear plots are shown when displaying $-\ln(C_o/C_t)$ against t, with correlation coefficients (R^2) of around 0.9700 for the RhB and 0.9914 for the MB. The reaction rate constant for RhB was 5.78×10^{-2} min^{-1} and for MB it was 9.62×10^{-2} min^{-1}, demonstrating TPA-TAZ HPP has better photocatalytic performance for MB than RhB [Figs. 5(c) and 5(e)]. These results show our novel TPA-TAZ HPP exhibits the highest reaction rate constant for dyes than other reported photocatalyst as Py-CMP-1 (2×10^{-2} min^{-1}) [46], Py-CMP-2 (3.4×10^{-2} min^{-1}) [46], TFP-BF 3DCOF (1.5×10^{-2} min^{-1}) [48], TFP-Py 3D COF (1.1×10^{-2} min^{-1}) [48], $Bi_4Ti_3O_{12}$ (1.6×10^{-2} min^{-1}) [52], TPPDA-Py CMP (3.3×10^{-2} min^{-1}) [57], and TPPDA-TBP CMP (2.1×10^{-2} min^{-1}) [57]. Recycling and recycling was crucial for controlling secondary pollutants and for economic use. The reusability of TPA-TAZ HPP in RhB and MB degradation was therefore examined across ten cycles in similar conditions. Strong photocatalytic activity was maintained by the TPA-TAZ HPP, which reduced MB by 8.78 % and RhB by 7.77 % [Fig. 5(f)]. Furthermore, FTIR spectra recorded before and after photodegradation showed no significant changes in the characteristic bands, with only minor shifts in wavenumbers. These observations support our earlier assumption regarding the presence of interfacial π–π stacking interactions between the adsorbent and dye molecules [Figure S9].

A detailed analysis of TPA-TAZ HPP was conducted to identify the reactive radicals involved in its photodegradation process. The proposed mechanism is illustrated in [Fig. 6 (a)]. Upon light irradiation, electrons in TPA-TAZ HPP are excited to the LUMO, while positive charges remain in the HOMO. These electrons can react with O_2 to generate $\bullet O_2$ radicals [62,63]. The photogenerated holes in the HOMO exhibit strong oxidation potential to produce •OH radicals, directly contributing to the photocatalytic degradation of RhB and MB [63]. Additionally, •OH radicals may also form through a two-electron oxidation process involving electrons in the LUMO, as reported in previous studies. The activated oxygen species ($\bullet O_2$) can further interact with electrons to produce •OH radicals. The overall reaction pathway is summarized in the following Eqs. (1–6)→.

$$\text{TPA-HPP} + \text{Sunlight} \rightarrow e^+ + H^+ \quad (1)$$

$$H_2O \rightarrow O_2 + H^+ \quad (2)$$

$$O_2 + e^- \rightarrow \bullet O_2^- \quad (3)$$

$$\bullet O_2^- + e^- + H_2O \rightarrow \bullet OH + OH^- \quad (4)$$

$$\text{Dyes} + \bullet O_2^-/\bullet \rightarrow \text{OH } CO_2 + H_2O \quad (5)$$

$$\text{Dyes} + h^+ \rightarrow CO_2 + H_2O \quad (6)$$

To gain mechanistic insights into the photodegradation process, electron paramagnetic resonance (EPR) spectroscopy using specific spin traps to identify the active species involved, under both dark and light conditions [Fig. 6 (b-d)]. The photoexcited electrons in the LUMO of TPA-TAZ HPP react with dissolved molecular oxygen (O_2), forming

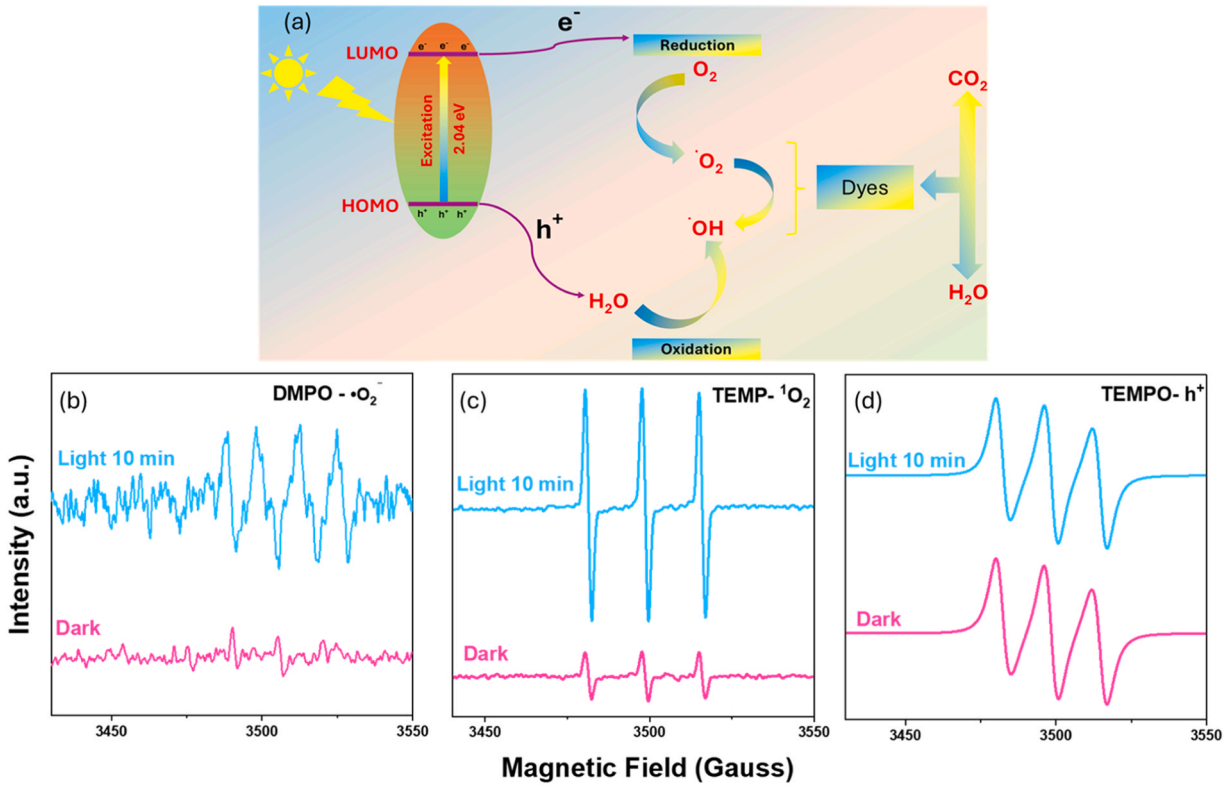

Fig. 6. (a) Proposed photodegradation mechanism of dyes using TPA-TAZ HPP. EPR signals for (b) $\bullet O_2^-$ (c) $^1O_2$ and (d) h^+.

superoxide radicals ($\bullet O_2^-$). The presense of superoxide radicals ($\bullet O_2^-$) was confirmed using 5,5-dimethyl-1-pyrroline *N*-oxide (DMPO) as spin trap. No characteristic EPR signals for $\bullet O_2^-$ are observed in the dark; however, upon light exposure, distinct and progressively intense signals appear with increasing irradiation time, confirming the light-induced formation and accumulation of $\bullet O_2^-$ radicals on the surface of TPA-TAZ HPP [Fig. 6 (b)]. In addition, singlet oxygen ($^1O_2$) generation was confirmed using 2,2,6,6-tetramethylpiperidine (TEMP) as a spin trap. The corresponding EPR signal intensity increased significantly under illumination compared to dark conditions, validating the photo-induced formation of $^1O_2$ [Fig. 6 (c)]. Both $\bullet O_2^-$ and $^1O_2$ are known to attack the chromophoric structures of dyes, breaking down key bonds such as C═C, C–N, and N = N, and leading to decolorization and mineralization. To evaluate the role of photogenerated holes (h^+), 2,2,6-trimethylpiperidine-1-oxyl (TEMPO) was used as a spin trap. However, no noticeable change in the EPR signal intensity was observed under either dark or light conditions, suggesting that h^+ are not significantly involved in direct dye oxidation or may rapidly recombine with electrons [Fig. 6 (d)]. Furthermore, the absence of a hydroxyl radical (•OH) signal indicates that •OH does not play a major role in the degradation process. These observations strongly support a ROS-mediated photodegradation pathway predominantly involving superoxide and singlet oxygen species, enabled by the tailored electronic structure and charge dynamics of the TPA-TAZ HPP photocatalyst. This mechanism underscores the material's promising potential for advanced wastewater treatment through efficient and selective dye degradation.

The enhanced photodegradation performance of dyes using the synthesized porous TPA-TAZ HPP structure can be attributed to its optimal charge separation and hole mobility. Under visible light irradiation, dye molecules such as Methylene Blue (MB) and Rhodamine B (RhB) become photoexcited, promoting electrons from their HOMO to LUMO levels. Given the favorable band alignment, these excited electrons can readily transfer from the LUMO of MB (0.065 V vs. NHE) and RhB (0.58 V vs. NHE) [64] to the significantly lower LUMO of TPA-TAZ HPP (–3.83 V vs. NHE), allowing efficient electron trapping. Concurrently, the HOMO level of TPA-TAZ HPP (–1.79 V vs. NHE) lies below the HOMO levels of MB (1.77 V vs. NHE) and RhB (2.78 V vs. NHE), which favors hole migration from the polymer to the dye molecules enabling effective electron trapping [Fig. 7]. This synergistic electron–hole transfer mechanism not only facilitates spatial charge separation but also enhances the generation of reactive oxygen species (ROS), accelerating the degradation of dye molecules. The favorable alignment of the bandgap and energy levels (HOMO and LUMO) of TPA-TAZ HPP underscores its strong potential for photocatalytic wastewater treatment.

4. Conclusions

In summary, we successfully synthesized donor–acceptor-based TPA-TAZ HPP via Friedel−Crafts polymerization for dual applications in both physisorption and photodegradation of organic dyes in water. The resulting TPA-TAZ HPP exhibited an impressive surface area and excellent thermal stability (T_{d5}: 663 °C, T_{d10}: 674 °C) with a high char yield of 75 %. The adsorption performance of TPA-TAZ HPP was remarkable, achieving rapid and efficient removal of RhB and MB within just 5 minutes. The Q_m were determined to be 951 mg g^{-1} for RhB and 858 mg g^{-1} for MB, surpassing or at least matching the performance of many previously reported porous materials under similar conditions. In addition to its high adsorption efficiency, TPA-TAZ HPP demonstrated a well-suited band gap arrangement and donor-acceptor configuration, which contributed to its outstanding photocatalytic activity. The material achieved photodegradation efficiencies of 88 % for RhB and 96 % for MB, with corresponding reaction rate constants of 5.78×10^{-2} min^{-1} and 9.62×10^{-2} min^{-1}, respectively. These values indicate that TPA-TAZ HPP is equivalent to, and may surpass, that of many conjugated polymers and COFs previously examined under similar photodegradation circumstances. Owing to these exceptional properties, TPA-TAZ HPP holds significant potential as an effective adsorbent and photocatalyst for water pollutant removal, making it a promising candidate for wastewater treatment and environmental remediation.

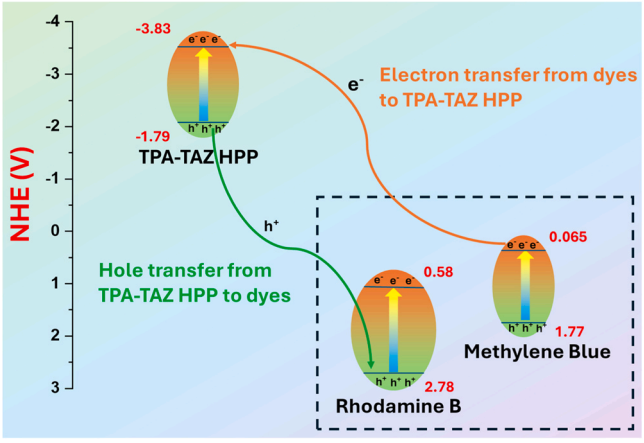

Fig. 7. (a) Possible charge transfer mechanism between TPA-TAZ HPP and dyes.

CRediT authorship contribution statement

Shiao-Wei Kuo: Supervision, Resources, Project administration, Funding acquisition. **Mohammed G. Kotp:** Validation, Data curation. **Ahmed M. Elewa:** Visualization, Validation, Data curation. **Mohsin Ejaz:** Writing – review & editing, Writing – original draft, Visualization, Validation, Software, Methodology, Data curation, Conceptualization. **Mohamed Gamal Mohamed:** Writing – review & editing, Writing – original draft, Visualization, Validation, Supervision, Investigation, Data curation, Conceptualization.

Declaration of Competing Interest

The authors declare that they have no known competing financial interests or personal relationships that could have appeared to influence the work reported in this paper.

Acknowledgements

This study was supported financially by the National Science and Technology Council, Taiwan, under contracts NSTC 113-2223-E-110–001- and 113–2221-E-110–012-MY3. The authors thank the staff at National Sun Yat-sen University for their assistance with the TEM (ID: EM022600) experiments.

Appendix A. Supporting information

Supplementary data associated with this article can be found in the online version at doi:10.1016/j.colsurfa.2025.137239.

Data availability

Data will be made available on request.

References

[1] Y. Tang, Y. Liu, Y. Chen, W. Zhang, J. Zhao, S. He, C. Yang, T. Zhang, C. Tang, C. Zhang, Z. Yang, A review: research progress on microplastic pollutants in aquatic environments, Sci. Total Environ. 766 (2021) 142572, https://doi.org/10.1016/j.scitotenv.2020.142572.

[2] S.U. Rehman, M. Farooq, A. Haleem, J. Ambreen, M. Siddiq, S.A. Althobaiti, Facile synthesis of highly macroporous Gum Arabic hydrophilic cryogel for dyes

adsorption, Int. J. Mod. Phys. B 38 (2024) 2450127, https://doi.org/10.1142/S0217979224501273.
[3] A. Issakhov, A. Alimbek, Y. Zhandaulet, The assessment of water pollution by chemical reaction products from the activities of industrial facilities: numerical study, J. Clean. Prod. 282 (2021) 125239, https://doi.org/10.1016/j.jclepro.2020.125239.
[4] R. Naidu, B. Biswas, I.R. Willett, J. Cribb, B. Kumar Singh, C. Paul Nathanail, F. Coulon, K.T. Semple, K.C. Jones, A. Barclay, R.J. Aitken, Chemical pollution: a growing peril and potential catastrophic risk to humanity, Environ. Int. 156 (2021) 106616, https://doi.org/10.1016/j.envint.2021.106616.
[5] B.S. Rathi, P.S. Kumar, D.-V.N. Vo, Critical review on hazardous pollutants in water environment: Occurrence, monitoring, fate, removal technologies and risk assessment, Sci. Total Environ. 797 (2021) 149134, https://doi.org/10.1016/j.scitotenv.2021.149134.
[6] A. Sahu, J.C. Poler, Removal and degradation of dyes from textile industry wastewater: benchmarking recent advancements, toxicity assessment and cost analysis of treatment processes, J. Environ. Chem. Eng. 12 (2024) 113754, https://doi.org/10.1016/j.jece.2024.113754.
[7] Ye Cheng, Y. Chen, M. He, N. Zhou, X. Meng, Z. Dai, Y. Xiong, Photo-tunable ultrafast removal of organic dyes by azobenzene and phosphonium functionalized porous organic polymers, Sep. Purif. Technol. 335 (2024) 126119, https://doi.org/10.1016/j.seppur.2023.126119.
[8] Y. Zhu, R. Ding, S. Chen, X. Qu, Y. Yang, X. Zhang, Three-dimensional sulfonic-functionalized porphyrin-based porous organic polymer for high-performance methylene blue and ciprofloxacin capture, Sep. Purif. Technol. 333 (2024) 125857, https://doi.org/10.1016/j.seppur.2023.125857.
[9] V. Vinayagam, K.N. Palani, S. Ganesh, S. Rajesh, V.V. Akula, R. Avoodaiappan, O. S. Kushwaha, A. Pugazhendhi, Recent developments on advanced oxidation processes for degradation of pollutants from wastewater with focus on antibiotics and organic dyes, Environ. Res. 240 (2024) 117500, https://doi.org/10.1016/j.envres.2023.117500.
[10] C.-W. Hsiao, A.M. Elewa, M.G. Mohamed, M.G. Kotp, M.M.-C. Chou, S.-W. Kuo, Designing strategically functionalized hybrid porous polymers with octavinylsilsesquioxane/dibenzo[g,p]chrysene/benzo[c]-1,2,5-thiadiazole units for rapid removal of Rhodamine B dye from water, Colloids Surf., A 699 (2024) 134658, https://doi.org/10.1016/j.colsurfa.2024.134658.
[11] M.F. Lanjwani, M. Tuzen, M.Y. Khuhawar, T.A. Saleh, Trends in photocatalytic degradation of organic dye pollutants using nanoparticles: a review, Inorg. Chem. Commun. 159 (2024) 111613, https://doi.org/10.1016/j.inoche.2023.111613.
[12] Z. Wu, Z. Zhu, J. Ma, M. Zhou, Z. Wu, H. You, H. Zhang, N. Li, F. Wang, High piezo-photocatalysis of $BaTiO_3$ nanofibers for organic dye decomposition, Surf. Interfaces 48 (2024) 104308, https://doi.org/10.1016/j.surfin.2024.104308.
[13] M. Qu, D. He, Z. Luo, R. Wang, F. Shi, Y. Pang, W. Sun, L. Peng, J. He, Facile preparation of a multifunctional superhydrophilic PVDF membrane for highly efficient organic dyes and heavy metal ions adsorption and oil/water emulsions separation, Colloids Surf., A 637 (2022) 128231, https://doi.org/10.1016/j.colsurfa.2021.128231.
[14] R. Imsong, D. Dhar Purkayastha, Dual-functional superhydrophilic/underwater superoleophobic 2D Ti_3C_2TX MXene-PAN membrane for efficient oil-water separation and adsorption of organic dyes in wastewater, Sep. Purif. Technol. 306 (2023) 122636, https://doi.org/10.1016/j.seppur.2022.122636.
[15] Y. Li, J. Zhang, S. Liu, C. Zhang, C. Chuah, Y. Tang, R.T.K. Kwok, J.W.Y. Lam, H. Ou, D. Ding, B.Z. Tang, Enlarging the reservoir: high absorption coefficient dyes enable synergetic near infrared-ii fluorescence imaging and near infrared-i photothermal therapy, Adv. Funct. Mater. 31 (2021) 2102213, https://doi.org/10.1002/adfm.202102213.
[16] C. Yin, X. Li, Y. Wang, Y. Liang, S. Zhou, P. Zhao, C.-S. Lee, Q. Fan, W. Huang, Organic semiconducting macromolecular dyes for NIR-II photoacoustic imaging and photothermal therapy, Adv. Funct. Mater. 31 (2021) 2104650, https://doi.org/10.1002/adfm.202104650.
[17] C.-W. Hsiao, A.M. Elewa, M.G. Mohamed, S.-W. Kuo, Highly stable hybrid porous polymers containing polyhedral oligomeric silsesquioxane (POSS)/Dibenzo[g,p] chrysene and Dibenzo[b,d]thiophene units for efficient Rhodamine B dye removal, Sep. Purif. Technol. 332 (2024) 125771, https://doi.org/10.1016/j.seppur.2023.125771.
[18] R. Agarwala, L. Mulky, Adsorption of dyes from wastewater: a comprehensive review, ChemBioEng Rev. 10 (2023) 326–335, https://doi.org/10.1002/cben.202200011.
[19] L. Hevira, J.O. Ighalo, D. Sondari, Chitosan-based polysaccharides for effective synthetic dye adsorption, J. Mol. Liq. 393 (2024) 123604, https://doi.org/10.1016/j.molliq.2023.123604.
[20] C. Wei, Y. Cai, Z. Yang, A bifunctional imidazolium-based porous organic polymer for efficient detection of $Cr_2O_7^{2-}$ and adsorptive separation of $Cr_2O_7^{2-}$ and MO in water, J. Water Process Eng. 57 (2024) 104573, https://doi.org/10.1016/j.jwpe.2023.104573.
[21] P. Saini, N. Chakinala, P.K. Surolia, A. Gupta Chakinala, Ultrasound-assisted enhanced adsorption of textile dyes with metal organic frameworks, Sep. Purif. Technol. 354 (2025) 128730, https://doi.org/10.1016/j.seppur.2024.128730.
[22] J. De Smedt, P.M. Heynderickx, P.J. Arauzo, F. Ronsse, Adsorption mechanism of different dyes on chemical activated carbon as quantitative assessment for wastewater treatment: comparative study between $ZnCl_2$ and its eutectic, Sep. Purif. Technol. 334 (2024) 126002, https://doi.org/10.1016/j.seppur.2023.126002.
[23] Z.M. Şenol, H. Arslanoğlu, Z.S. Keskin, V. Mehmeti, N. El Messaoudi, Biosorption of rhodamine B and sunset yellow dyes on cross-linked chitosan-alginate biocomposite beads: experimental and theoretical studies, Int. J. Biol. Macromol. 298 (2025) 139264, https://doi.org/10.1016/j.ijbiomac.2024.139264.
[24] M. Ejaz, M.G. Mohamed, S.-W. Kuo, Solid state chemical transformation provides a fully benzoxazine-linked porous organic polymer displaying enhanced CO_2 capture and supercapacitor performance, Polym. Chem. 14 (2023) 2494–2509, https://doi.org/10.1039/D3PY00158J.
[25] M. Ejaz, M.G. Mohamed, W.-C. Huang, S.-W. Kuo, Pyrene-based covalent organic polymers with nano carbonaceous composites for efficient supercapacitive energy storage, J. Mater. Chem. A 11 (2023) 22868–22883, https:// doi.org/10.1039/D3TA02741D.
[26] M. Ejaz, M.M. Samy, Y. Ye, S.-W. Kuo, M. Gamal Mohamed, Design hybrid porous organic/inorganic polymers containing polyhedral oligomeric silsesquioxane/pyrene/anthracene moieties as a high-performance electrode for supercapacitor, Int. J. Mol. Sci. (2023), https://doi.org/10.3390/ijms24032501.
[27] M. Ejaz, M.G. Mohamed, S.U. Sharma, J.-T. Lee, C.-F. Huang, T. Chen, S.-W. Kuo, An ultrastable porous polyhedral oligomeric silsesquioxane/tetraphenylthiophene hybrid as a high-performance electrode for supercapacitors, Molecules 27 (2022) 6238, https://doi.org/10.3390/molecules27196238.
[28] M. Ejaz, M.G. Mohamed, S.-W. Kuo, FluorescenT Benzoxazine–perylene Linked Covalent Organic Polymer as A Sensing Probe for Lead Ions and 2,4,6-trinitrophenol, ACS Appl. Polym. Mater. 6 (2024) 9170–9179, https:// doi.org/10.1021/acsapm.4c01514.
[29] H.-Y. Kong, T.-X. Wang, Y. Tao, X. Ding, B.-H. Han, Crown ether-based hypercrosslinked porous polymers for gold adsorption, Sep. Purif. Technol. 290 (2022) 120805, https://doi.org/10.1016/j.seppur.2022.120805.
[30] M. Ejaz, M.G. Mohamed, W.-C. Chang, S.-W. Kuo, Synthesis and design of hypercrosslinked porous organic frameworks containing tetraphenylpyrazine unit for high-performance supercapacitor, J. Polym. Sci. 62 (2024) 1629–1638, https://doi.org/10.1002/pol.20230174.
[31] M.G. Mohamed, A.M. Elewa, M.-S. Li, S.-W. Kuo, Construction and multifunctional of hypercrosslinked porous organic polymers containing ferrocene unit for high-performance iodine adsorption and supercapacitor, J. Taiwan Inst. Chem. Eng. 150 (2023) 105045, https://doi.org/10.1016/j.jtice.2023.105045.
[32] M.G. Mohamed, A.F.M. El-Mahdy, M.G. Kotp, S.-W. Kuo, Advances in porous organic polymers: syntheses, structures, and diverse applications, Mater. Adv. 3 (2022) 707–733, https://doi.org/10.1039/D1MA00771H.
[33] M.G. Mohamed, N.-Y. Liu, A.F.M. El-Mahdy, S.-W. Kuo, Ultrastable luminescent hybrid microporous polymers based on polyhedral oligomeric silsesquioxane for CO_2 uptake and metal ion sensing, Microporous Mesoporous Mater. 311 (2021) 110695, https://doi.org/10.1016/j.micromeso.2020.110695.
[34] S. Señorans, I. Valencia, E. Merino, M. Iglesias, M.A. Fernández-Rodríguez, E. M. Maya, Hyper-cross-linked porous polymer featuring B–N covalent bonds (HCP-BNs): a stable and efficient metal-free heterogeneous photocatalyst, ACS Macro Lett. 12 (2023) 949–954, https://doi.org/10.1021/acsmacrolett.3c00217.
[35] Y. Huang, G. Ruan, Y. Ruan, W. Zhang, X. Li, F. Du, C. Hu, J. Li, Hypercrosslinked porous polymers hybridized with graphene oxide for water treatment: dye adsorption and degradation, RSC Adv. 8 (2018) 13417–13422, https://doi.org/10.1039/C8RA01620H.
[36] G.E.M. Schukraft, R.T. Woodward, S. Kumar, M. Sachs, S. Eslava, C. Petit, Hypercrosslinked Polymers as a Photocatalytic Platform for Visible-Light-Driven CO_2 Photoreduction Using H_2O, ChemSusChem 14 (2021) 1720–1727, https://doi.org/10.1002/cssc.202002824.
[37] A. Waheed, N. Baig, N. Ullah, W. Falath, Removal of hazardous dyes, toxic metal ions and organic pollutants from wastewater by using porous hyper-cross-linked polymeric materials: a review of recent advances, J. Environ. Manag. 287 (2021) 112360, https://doi.org/10.1016/j.jenvman.2021.112360.
[38] M.G. Kotp, S.-W. Kuo, Harnessing solar energy with porous organic polymers: advancements, challenges, economic, environmental impacts and future prospects in sustainable photocatalysis, Mater. Today Chem. 41 (2024) 102299, https://doi.org/10.1016/j.mtchem.2024.102299.
[39] T. Zhang, G. Xing, W. Chen, L. Chen, Porous organic polymers: a promising platform for efficient photocatalysis, Mater. Chem. Front 4 (2020) 332–353, https://doi.org/10.1039/C9QM00633H.
[40] Z. Zhang, J. Jia, Y. Zhi, S. Ma, X. Liu, Porous organic polymers for light-driven organic transformations, Chem. Soc. Rev. 51 (2022) 2444–2490, https://doi.org/10.1039/D1CS00808K.
[41] J. Yu, X. Sun, X. Xu, C. Zhang, X. He, Donor-acceptor type triazine-based conjugated porous polymer for visible-light-driven photocatalytic hydrogen evolution, Appl. Catal., B 257 (2019) 117935, https://doi.org/10.1016/j.apcatb.2019.117935.
[42] K. Wu, X.-Y. Liu, M. Xie, P.-W. Cheng, J. Zheng, W. Lu, D. Li, Rational design of D− π − A− π − D porous organic polymer with polarized π for photocatalytic aerobic oxidation, Appl. Catal., B 334 (2023) 122847, https://doi.org/10.1016/j.apcatb.2023.122847.
[43] N. Saini, K. Dhingra, A. Kumar, K. Kailasam, Molecular structural engineering of donor–acceptor-based porous organic polymers for sulfide photooxidation in water: a sustainable approach, Green. Chem. 26 (2024) 10314–10323, https://doi.org/10.1039/D4GC03255A.
[44] R. Sang, Y. Hu, Z. Shen, G. Zhao, J. Yue, X. Huang, Low-temperature synthesis of porous organic polymers with donor–acceptor structure and β-ketoenamine for photocatalytic oxidative coupling of amines, Nanoscale 16 (2024) 8931–8940, https://doi.org/10.1039/D4NR00391H.
[45] X. Wang, C. Wang, H.-Q. Tan, T.-Y. Qiu, Y.-M. Xing, Q.-K. Shang, Y.-N. Zhao, X.-Y. Zhao, Y.-G. Li, Design of porous organic polymer photocatalysts based on heptazine for efficient photocatalytic aerobic oxidation, Chem. Eng. J. 431 (2022) 134051, https://doi.org/10.1016/j.cej.2021.134051.

[46] I. Nath, J. Chakraborty, P.M. Heynderickx, F. Verpoort, Engineered synthesis of hierarchical porous organic polymers for visible light and natural sunlight induced rapid degradation of azo, thiazine and fluorescein based dyes in a unique mechanistic pathway, Appl. Catal. B Environ. 227 (2018) 102–113, https://doi.org/10.1016/j.apcatb.2018.01.032.

[47] H.L. Wang, F.G. Xi, X.Y. Xu, Y.Q. Yan, J.Y. Sun, X. Luo, P. Gu, S. Zhou, Construction of a platform to develop 3D ionic porous organic polymers via a post-modification strategy for efficient adsorption of charged organic pollutants, Sep. Purif. Technol. 360 (2025) 131124, https://doi.org/10.1016/j.seppur.2024.131124.

[48] Z. Zhong, X. Xia, X. Yang, N. Li, J. He, D. Chen, P. Gu, Q. Xu, J. Lu, Metal-free modification of porphyrin-based porous organic polymers for effective photocatalytic degradation of bisphenol A in water, Sep. Purif. Technol. 301 (2022) 121981, https://doi.org/10.1016/j.seppur.2022.121981.

[49] M. Salahvarzi, A. Setaro, S. Beyranvand, M. Nemati, G. Gordeev, A. Fiebor, K. Ludwig, R. Ghanbari, N. Nasiri, V. Ahmadi, M. Weber, Z. Jamshidi, C. Cheng, S. Reich, M. Adeli, Room temperature synthesis of triazine covalent organic frameworks for size-selective intercalation of molecules and fast water purification, Mater. Today Chem. 39 (2024) 102155, https://doi.org/10.1016/j.mtchem.2024.102155.

[50] N. Pritee, S. Dhariwal, S. Yadav, S. Sharma, Thakur, Enhanced photocatalytic degradation of environmental pollutants using a triphenylamine-based polymer: synthesis, characterization, and mechanistic insights, Langmuir 40 (2024) 26007–26017, https://doi.org/10.1021/acs.langmuir.4c03461.

[51] P. Ren, X. Ren, J. Xu, H. Li, Y. Zheng, Y. Hong, Y. Lin, Y. Zhou, Y. Chen, W. Zhang, Excellent adsorption property and mechanism of oxygen vacancies-assisted hexagonal MoO_3 nanosheets for methylene blue and rhodamine b dyes, Appl. Surf. Sci. 597 (2022) 153699, https://doi.org/10.1016/j.apsusc.2022.153699.

[52] T. Cheng, X. Sun, T. Xian, Z. Yi, R. Li, X. Wang, H. Yang, Tert-butylamine/oleic acid-assisted morphology tailoring of hierarchical $Bi_4Ti_3O_{12}$ architectures and their application for photodegradation of simulated dye wastewater, Opt. Mater. 112 (2021) 110781, https://doi.org/10.1016/j.optmat.2020.110781.

[53] Y. Zhuang, Q. Zhu, G. Li, Z. Wang, P. Zhan, C. Ren, Z. Si, S. Li, D. Cai, P. Qin, Photocatalytic degradation of organic dyes using covalent triazine-based framework, Mater. Res. Bull. 146 (2022) 111619, https://doi.org/10.1016/j.materresbull.2021.111619.

[54] N. Klomkliang, D.D. Do, D. Nicholson, Effects of temperature, pore dimensions and adsorbate on the transition from pore blocking to cavitation in an ink-bottle pore, Chem. Eng. J. 239 (2014) 274–283, https://doi.org/10.1016/j.cej.2013.11.019.

[55] P.T.M. Nguyen, C. Fan, D.D. Do, D. Nicholson, On the cavitation-like pore blocking in ink-bottle pore: evolution of hysteresis loop with neck size, J. Phys. Chem. C. 117 (2013) 5475–5484, https://doi.org/10.1021/jp4002912.

[56] D. Zhang, L. Tao, Q. Wang, T. Wang, A facile synthesis of cost-effective triphenylamine-containing porous organic polymers using different crosslinkers, Polymers 82 (2016) 114–120, https://doi.org/10.1016/j.polymer.2015.11.041.

[57] M.G. Kotp, C.-L. Chang, A.F.M. El-Mahdy, Tetraphenyl-p-phenylenediamine-based tunable conjugated microporous polymers: adsorption and photodegradation of hazardous dyestuff in aqueous environments, J. Water Process Eng. 53 (2023) 103675, https://doi.org/10.1016/j.jwpe.2023.103675.

[58] S. Han, Z. Li, S. Ma, Y. Zhi, H. Xia, X. Chen, X. Liu, Bandgap engineering in benzotrithiophene-based conjugated microporous polymers: a strategy for screening metal-free heterogeneous photocatalysts, J. Mater. Chem. A 9 (2021) 3333–3340, https://doi.org/10.1039/D0TA10232F.

[59] L. Jing, P. Li, Z. Li, D. Ma, J. Hu, Influence of π–π interactions on organic photocatalytic materials and their performance, Chem. Soc. Rev. 54 (2025) 2054–2090, https://doi.org/10.1039/D4CS00029C.

[60] Y. Wang, X. Cui, P. Zhang, Y. Wang, W. Lu, Synthesis of porphyrin porous organic polymers and their application of water pollution treatment: a review, Environ. Technol. Innov. 29 (2023) 102972, https://doi.org/10.1016/j.eti.2022.102972.

[61] S. Zhou, L. Jin, P. Gu, L. Tian, N. Li, D. Chen, A. Marcomini, Q. Xu, J. Lu, Novel calixarene-based porous organic polymers with superfast removal rate and ultrahigh adsorption capacity for selective separation of cationic dyes, Chem. Eng. J. 433 (2022) 134442, https://doi.org/10.1016/j.cej.2021.134442.

[62] Y. Cao, Y. Ren, J. Zhang, T. Xie, Y. Lin, Activation of H_2O_2 by photo-generated electrons for enhanced visible light driven methylene blue degradation with $ZnFe_2O_4/BiVO_4$ heterojunction, Opt. Mater. 121 (2021) 111637, https://doi.org/10.1016/j.optmat.2021.111637.

[63] M.A. Kanjwal, K.K.S. Lo, W.W.-F. Leung, Graphene composite nanofibers as a high-performance photocatalyst for environmental remediation, Sep. Purif. Technol. 215 (2019) 602–611, https://doi.org/10.1016/j.seppur.2019.01.044.

[64] A. Lebedev, F. Anariba, X. Li, P. Wu, Rational design of visible-light-sensitive Ag-BiVO4 oxides by matching redox potentials of catalyst, dyes, and reactive oxygen species towards more efficient photocatalytic degradation, J. Environ. Chem. Eng. 8 (2020) 103748, https://doi.org/10.1016/j.jece.2020.103748.